Geophys. J. Int. (2016) **205,** 681–693
Advance Access publication 2016 February 8
GJI Seismology
doi: 10.1093/gji/ggw045

Tidal stress triggering of earthquakes in Southern California

Magda Bucholc[1] and Sandy Steacy[2]

[1]*School of Environmental Sciences, Ulster University, Cromore Road, Coleraine* BT52 1SA, *United Kingdom. E-mail: bucholc-m@email.ulster.ac.uk*
[2]*School of Physical Sciences, University of Adelaide, Adelaide SA* 5005, *Australia*

Accepted 2016 January 25. Received 2016 January 14; in original form 2015 August 9

SUMMARY

We analyse the influence of the solid Earth tides and ocean loading on the occurrence time of Southern California earthquakes. For each earthquake, we calculate tidal Coulomb failure stress and stress rate on a fault plane that is assumed to be controlled by the orientation of the adjacent fault. To reduce bias when selecting data for testing the tide-earthquake relationship, we create four earthquake catalogues containing events within 1, 1.5, 2.5 and 5 km of nearest faults. We investigate the difference in seismicity rates at times of positive and negative tidal stresses/stress rates given three different cases. We consider seismicity rates during times of positive versus negative stress and stress rate, as well as 2 and 3 hr surrounding the local tidal stress extremes. We find that tidal influence on earthquake occurrence is found to be statistically non-random only in close proximity to tidal extremes meaning that magnitude of tidal stress plays an important role in tidal triggering. A non-random tidal signal is observed for the reverse events. Along with a significant increase in earthquake rates around tidal Coulomb stress maxima, the strength of tidal correlation is found to be closely related to the amplitude of the peak tidal Coulomb stress (τ_p). The most effective tidal triggering is found for $\tau_p \geq 1$ kPa, which is much smaller than thresholds suggested for static and dynamic triggering of aftershocks.

Key words: Time-series analysis; Tides and planetary waves; Earthquake dynamics; Seismicity and tectonics.

1 INTRODUCTION

One of the fundamental issues in seismology involves the determination and understanding of the conditions under which earthquake triggering can occur. Due to relatively slow tectonic loading ($\sim$0.1 kPa yr^{-1} or less), regional stresses remain incrementally below the local failure thresholds for tens to hundreds of years (Hill & Prejean 2013). Thus, insight into how earthquakes interact depends greatly on the analysis of short-term stress fluctuations.

Numerous studies try to relate a variety of phenomena that cause transient or periodic loading of the Earth's crust to triggered seismicity. The natural forcing functions generally fall into three categories: (1) static stress triggering, (2) quasi-static stress triggering and (3) dynamic stress triggering. Static stress changes, commonly expressed in terms of a change in the Coulomb Failure Function, perturb the stress field in the close vicinity of a fault. It has been demonstrated that static stress perturbations as low as 10 kPa (0.1 bar) can enhance or diminish the tectonic load on nearby faults (King *et al*. 1994; Hardebeck *et al*. 1998). Not only do spatial patterns of static stress changes seem to correspond well with the spatial distribution of aftershocks (Lasocki *et al*. 2009) but they also appear to explain seismic quiescence in the regions that were previously seismically active (Stein *et al*. 1997). In contrast to the static stress changes that develop concurrently with the earthquake rupture, quasi-static stress triggering results from stress changes that occur gradually over a period of years or decades. Here, change in the stress state is associated with slow, viscous relaxation of the lower-crust and upper mantle (Freed & Lin 2001; Pollitz & Sacks 2002). At greater distances from a main shock, where static and quasi-static stress changes become negligible, triggering is more likely to be caused by dynamic stress fluctuations generated by seismic waves propagating through the Earth's crust. Following the 1992 Landers event, increased seismicity rates were recorded throughout western North America at distances ranging from 200 to 1250 km that is well beyond the aftershock zone (Gomberg 1996). Dynamic triggering has also been observed after the passage of waves from the 1999 Hector Mine earthquake (Gomberg *et al*. 2001), the 2002 Denali earthquake (Gomberg *et al*. 2004), the 2004 Sumatra earthquake (West *et al*. 2005) and the 2011 Tohoku-Oki earthquake (Gonzalez-Huizar *et al*. 2012).

Along with dynamic stress changes induced by an earthquake rupture, dynamic stress fluctuations are continuously produced by lunar-solar attraction forces. Earth tides nudge the local stress field further from and closer to failure without permanently altering the net load on a fault. Since the amplitude of tidal stresses ($\sim$1 kPa) is a few orders of magnitude smaller than the average earthquake stress drop ($\sim 10^3$–10^4 kPa), they cannot supply the energy liberated in the earthquake (Scholz 2002). However, when superimposed on

tectonic stresses, tidal stresses could at times trigger an earthquake if the focal area stresses reached a critical value. Detection of the tidal signal (or its lack) could therefore provide valuable information on what conditions initiate a fault rupture. If the earthquake indeed occurs immediately after a critical level of stress has been reached, then we would expect more events to happen at times of tidal maxima. Measurements of tidal triggering due to different amplitudes of stresses could also help to estimate a low-amplitude reference point for spectrum of stresses capable of dynamic triggering.

Due to the completely predictable nature of tidal stresses, researches have attempted to measure the level of tidal triggering repeatedly. However, clear evidence of tidally triggered seismicity has not been detected as widely as might be expected. Finding the tidal signal in complex or limited data sets is challenging and many studies do not pay enough attention to statistical rigor (Emter 1997). There seems to be a tendency for positive results for regional catalogues and specific focal mechanisms (Shirley 1988; Wilcock 2001; Tanaka *et al*. 2004; Wilcock 2009) in contrast to global data sets (Heaton 1982; Curchin & Pennington 1987; Hartzell & Heaton 1989). Tanaka *et al*. (2002a) detect a particularly strong correlation between tidal shear stresses and 2800 globally distributed reverse fault events. The global study by Cochran *et al*. (2004) shows temporal patterns of tidal triggering for shallow-dipping thrust events and suggests that tidal correlations increase with the successively higher amplitudes of a periodic signal. Furthermore, the tidal triggering effect is observed for normal fault events by relating earthquake occurrence times to the time functions of the cubic tidal stress (Tsuruoka *et al*. 1995; Wilcock 2001) and vertical ground displacement (Métivier *et al*. 2009). No corresponding triggering effect is, however, detected for strike-slip events (Vidale *et al*. 1998).

Attempts have also been made to test the relationship between specific moon phases and earthquake occurrence. For example, Hartzell & Heaton (1989) searched for a fortnightly tidal periodicity in the Southern California and global earthquake catalogue, however, no such periodicity was observed. On the other hand, Iwata (2002) and Iwata & Young (2005) demonstrated that fluctuations of tidal stresses at times of full/new moon correlate with increased activity of acoustic emissions. The *b*-values of acoustic emissions were found to be significantly higher just after the times of full/new moon suggesting that *b*-values become larger during periods of high stresses.

A standard approach to examining the level of tidal triggering involves use of the Schuster statistic (Tanaka *et al*. 2002b; Cochran *et al*. 2004; Stroup *et al*. 2007; Tanaka 2012). It searches for periodicity in a data set by assessing the departure from randomness in the distribution of tidal phase angles. The tidal phase angle θi of the ith event is represented by its time of occurrence with respect to two subsequent maxima (or minima) of the tidal stress. In the Schuster test, each event is characterized by a unit vector, the orientation of which is defined by its tidal phase angle. The sum of all unit vectors is denoted by the resultant R. The probability p that a random set of n tidal phases will produce a vector sum whose magnitude is equal to or larger than R is given by

$$p = \exp\left(\frac{-R^2}{n}\right), \tag{1}$$

where R is the length of the vectorial sum and n is the total number of earthquakes (Heaton 1982). The p value corresponds to the significance level to reject the null hypothesis that earthquakes occur at random, that is, irrespective of the phase angle. The lower the p value is, the more convincing the evidence is against the null hypothesis and the higher the probability that the distribution of earthquakes stacked over the period T is non-uniform. However, it is important to note that the tidal signal has complicated features. It represents several tidal constituents with various periodicities (∼year, month, half month, day, half day etc.) which, when combined, give an endlessly varying aggregate. Due to constantly changing configurations of these periodic components, the time interval between two subsequent maxima/minima varies and in effect, tidal phases determined by interpolation do not have the same meaning for all the earthquakes. The correct and defendable use of the Shuster test depends thus on deciding which of these periodicities are to be examined. Nevertheless, decomposing the tidal signal into its basic components is not necessarily relevant since the extrema of individual tidal constituents are not always extrema of the total tidal signal. Here, we focus on the influence of the total periodic signal. In order to examine tidal periodicity of the earthquake time-series we do not implement the Schuster test but use the two-rate Poisson model which is commonly used to compare the occurrence rates of a given phenomenon in a specified time interval (Gu *et al*. 2008).

2 DATA AND METHOD OF INVESTIGATION

To assess whether tidal stresses modulate seismicity rates, we use earthquakes recorded by the Southern California Seismic Network (SCSN) between 1972 and 2013 in an area bounded by 114.5°W $< \varphi <$ 121.5°W and 31°N $< \lambda <$ 38°N. Following Tsuruoka *et al*. (1995), we believe that increasing tidal shear stress with simultaneous reduction of tidal normal pressure on a fault may have the largest effect on earthquake triggering. However, it is not always possible to uniquely distinguish between the fault plane and the auxiliary plane given an earthquake focal mechanism solution. While shear stresses on the two orthogonal nodal planes are the same due to the symmetry of the stress tensor, calculating the effect of normal stresses essentially depends on determining which nodal plane is the fault. Due to the ambiguity in identifying the fault plane, the tidal normal stresses very often cannot be calculated and used in further analysis (e.g. Tanaka *et al*. 2002a). To overcome this, we make an assumption that the failure plane is controlled by the orientation of its nearby adjacent fault. We use the geometry of 76 Southern California faults characterized by their strike, dip and rake angle (Petersen *et al*. 1996, 2008). The strike of simple segments of each fault is determined from the fault trace and dip direction. To avoid selection bias when choosing a data set for testing the tide-earthquake relationship, we consider four different earthquake catalogues: (1) Catalogue I including events within 1 km of the fault surface; (2) Catalogue II including events within 1.5 km of the fault surface; (3) Catalogue III including events within 2.5 km of the fault surface; (4) Catalogue IV including events within 5 km of the fault surface (Fig. 1). An estimate of completeness magnitude (M_c) for each catalogue is computed as a function of time using the MAXC technique (Wiemer & Wyss 2000); the charts are shown in Fig. 2. The MAXC method, in contrast to other methods, has the advantage of reaching a stable solution when applied to a limited data set (Mignan *et al*. 2011). The uncertainties in M_c are measured by using a Monte Carlo approximation of the bootstrap sampling method (Chernick 2007). Taking into account the temporal changes of M_c, we conclude that all four studied catalogues are complete for $M_c \geq 2.5$.

The significance of our observations is evaluated against the two-rate Poisson model (Vidale *et al*. 1998; Gu *et al*. 2008). The model is based on the assumption that earthquake frequency follows the

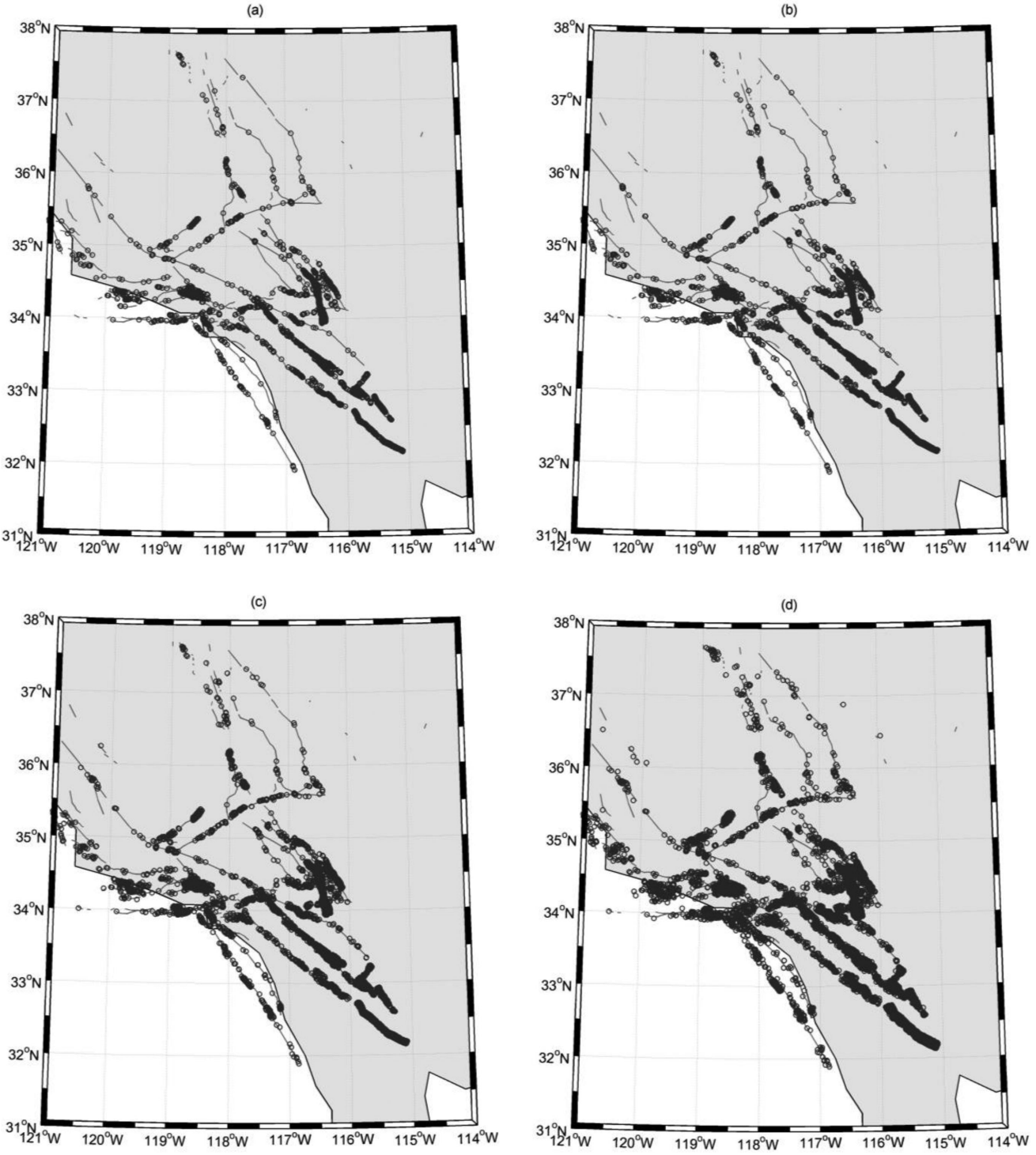

Figure 1. Maps of seismic activity along 76 geological structures for four earthquake catalogues used in this study. (a) Catalogue I includes the events within 1 km of the fault surface; (b) Catalogue II includes the events within 1.5 km of the fault surface; (c) Catalogue III includes the events within 2.5 km of the fault surface; (d) Catalogue IV includes the events within 5 km of the fault surface. The earthquake data have been obtained from the Southern California Earthquake Data Center (SCEDC) and cover the period 1972–2013.

Poisson distribution, in which the temporal variation in seismicity is purely due to a random process and the cumulative probability distribution of the time between successive events is exponential (Ayyub & McCuen 2011). This hypothesis has been regularly employed in seismic hazard analyses (e.g. Ashtari Jafari 2010; Wang *et al*. 2012); however, most of hazard estimation models have not addressed aftershock impact in their assessment. As pointed out by Gardner & Knopoff (1974) and Kagan & Jackson (1991), aftershock clusters are in fact non-Poissonian and only main-shock occurrence can be modelled satisfactorily as a realization of a Poisson process. Thus, several techniques have been proposed for removing dependent earthquakes that form seismicity clusters (e.g. Gardner & Knopoff

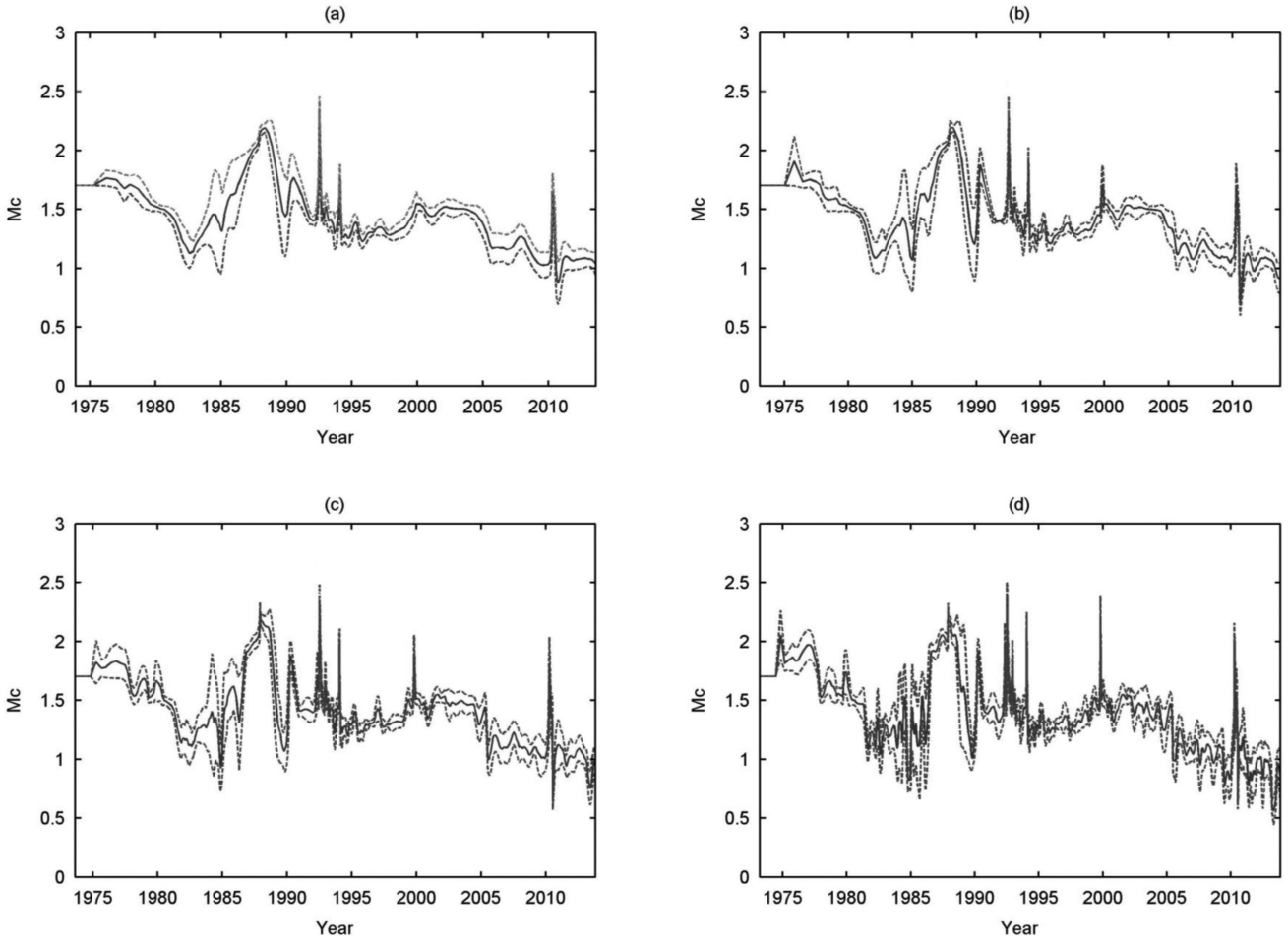

Figure 2. Magnitude of completeness (M_c) as a function of time for events recorded along 76 faults used in this analysis: (a) earthquakes within 1 km from the fault surface; (b) earthquakes within 1.5 km from the fault surface; (c) earthquakes within 2.5 km from the fault surface; (d) earthquakes within 5 km from the fault surface. M_c is evaluated using the MAXC technique (Wiemer & Wyss 2000). Dashed curves represent standard deviation $\pm\sigma$ obtained from 100 bootstrap samples. Moving window approach is used with a window of 1000 events.

1974; Reasenberg 1985; Zhuang *et al*. 2002). For the purpose of our analysis, we apply the linked-window method by Reasenberg (1985) that has been customarily used in the tidal-triggering studies (Hartzell & Heaton 1989; Wilcock 2001; Tanaka *et al*. 2002a). As a result of the declustering procedure, the events that are closely related to each other spatially or temporally are removed and accordingly, the numbers of earthquakes in the declustered Catalogues I, II, III and IV are 2193, 2990, 4469 and 6857 events, respectively. The cumulative frequency plots for the original and declustered catalogues are shown in Fig. 3.

To test the effect of tidal triggering on different types of focal mechanisms, we classify faults based on a 90° rake separation rule (Yang *et al*. 2012). Events with the rake angle in the 45° to 135° range are considered to be reverse faulting, events with rake angles from −45° to −135° exhibit normal faulting and events with any other rake angle are considered strike-slip. The style of faulting and the corresponding percentage and absolute number of earthquakes are summarized in Table 1.

Given the epicentral location and origin time of each event, we calculate the tidally induced strains using the GOTIC2 processing package (Matsumoto *et al*. 2001). Note that there are also other packages, such as SPOTL (Agnew 2012) or ETERNA 3.30 (Wenzel 1996), that are used for tidal analysis and prediction. Since several studies show that tidal triggering is more likely to be caused by a combined effect of solid tides and ocean loading rather than solid tides only (Tsuruoka *et al*. 1995; Wilcock 2001), we incorporate the loading effect into our calculations. In consequence, the contributions from solid earth tides and ocean tidal loading are computed for 16 short-period (M2, S2, K1, O1, N2, P1, K2, Q1, M1, J1, OO1, 2N2, Mu2, Nu2, L2 and T2) and 5 long-period (Mtm, Mf, Mm, Ssa and Sa) constituents for each earthquake time and location. The ocean tidal effect is estimated using the NAO99.b global ocean model based on 5 yr data from the TOPEX/POSEIDON satellite altimeter (Matsumoto *et al*. 2000; Takanezawa *et al*. 2001).

Having the non-zero, independent components of the strain tensor, $\varepsilon_{\theta\theta}$, $\varepsilon_{\varphi\varphi}$, $\varepsilon_{\theta\varphi}$ and ε_{rr} for each earthquake location, where θ is latitude north, φ is longitude east and r refers to radial direction, we calculate the stress tensor using the generalized form of Hooke's law:

$$\sigma = \lambda\,(\nabla \cdot u)\,I + 2\mu\varepsilon, \tag{2}$$

where σ is the stress tensor, $\nabla \cdot u$ is the divergence of the displacement vector u (where $\nabla \cdot u = \varepsilon_{\theta\theta} + \varepsilon_{\varphi\varphi} + \varepsilon_{rr}$ in spherical polar coordinates), I is the unit matrix, ε is the strain tensor, and λ and μ are the Lamè's parameters (Ranalli 1995). Positive $\varepsilon_{\theta\theta}$, $\varepsilon_{\varphi\varphi}$ and ε_{rr} refer to extension, positive $\varepsilon_{\theta\varphi}$ refers to right-lateral shear and the principal strain component in radial direction ε_{rr} is derived

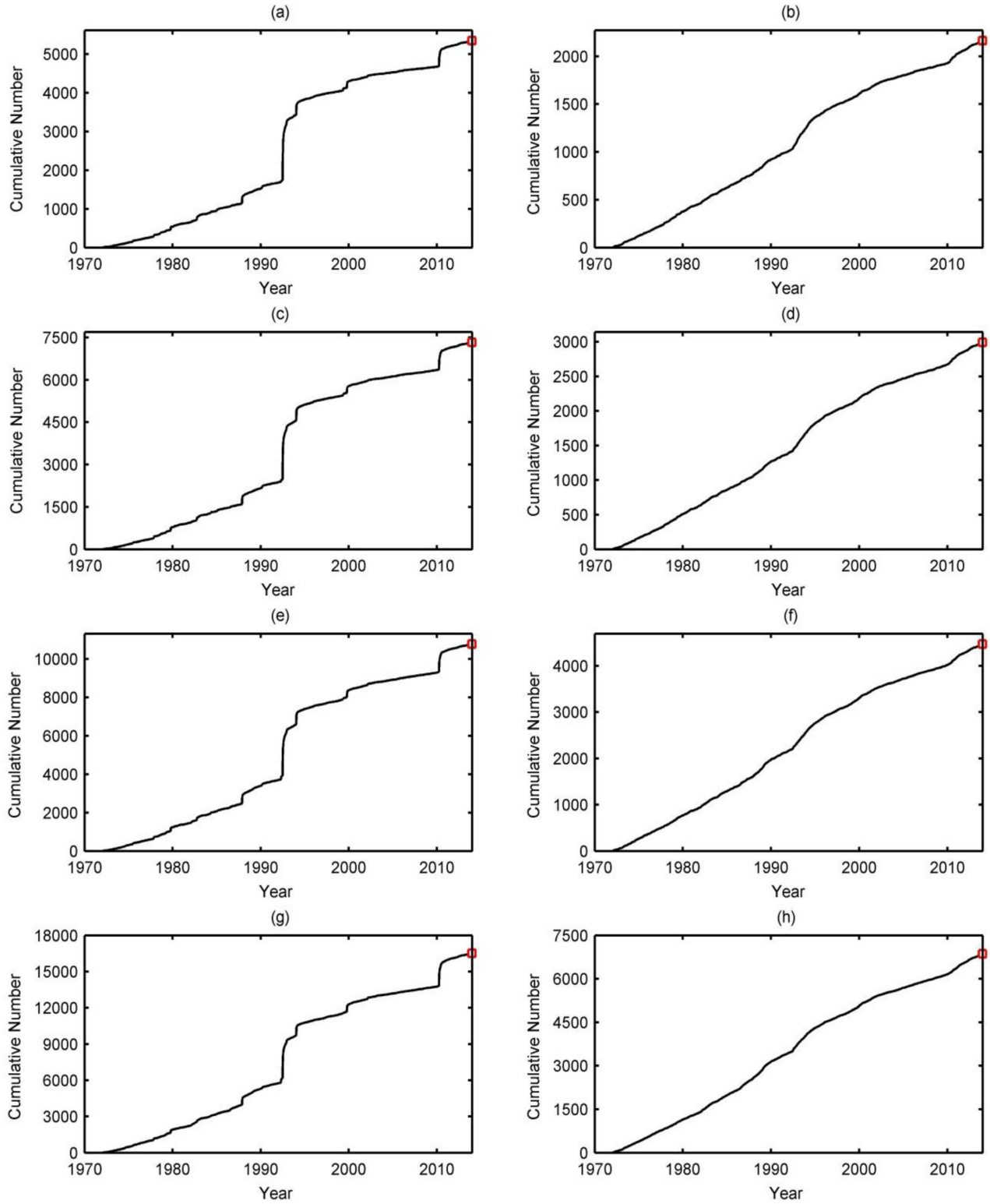

Figure 3. Cumulative temporal distribution of events in Southern California from 1972 to 2013 with completeness magnitude of 2.5, before and after declustering: the (a) non-declustered Catalogue I (5354 events); (b) declustered Catalogue I (2193 events); (c) non-declustered Catalogue II (7330 events); (d) declustered Catalogue II (2990 events); (e) non-declustered Catalogue III (10779 events); (f) declustered Catalogue III (4469 events); (g) non-declustered Catalogue IV (16526 events); (h) declustered Catalogue IV (6857 events). The algorithm of Reasenberg (1985) has been used for seismicity declustering.

from the volumetric strain ε_v. Elastic constants are consistent with $V_s = 3.20\,\mathrm{km\,s^{-1}}$, $V_p = 5.82\,\mathrm{km\,s^{-1}}$ and $\rho = 2600\,\mathrm{kg\,m^{-3}}$.

In order to examine how important tidal contribution might be in promoting or discouraging slip on the fault, we look at the Coulomb failure criterion as a function of tidal normal and shear stresses acting on a fault. Given a value of the tidal Coulomb stress, we can estimate if the fault has been brought further away, or closer to failure. For each event location and

Table 1. Data summary of the style of faulting for four earthquake catalogues used in this study.

Fault type	Catalogue I		Catalogue II		Catalogue III		Catalogue IV	
	N	% of all	*N*	% of all	*N*	% of all	*N*	% of all
Strike-slip	1790	81.6	2454	82.1	3648	81.6	5567	81.2
Reverse	380	17.3	503	16.8	766	17.1	1175	17.1
Normal	23	1.0	33	1.1	55	1.2	115	1.7
Total	2193	100.0	2990	100.0	4469	100.0	6857	100.0

time, we calculate Tidal Coulomb Failure Stress (TCFS) expressed as

$$\mathrm{TCFS} = \tau + \mu * \sigma_n, \tag{3}$$

where τ and σ_n are the tidal shear and normal stresses respectively, and μ is the effective coefficient of friction (e.g. King *et al*. 1994). Positive σ_n describes extension and positive value of τ refers to shear stress acting in the slip direction. We have considered a range of friction coefficients ($\mu = 0.2$, 0.4 and 0.6) and found that tidal correlation with earthquake timing is apparent for $\mu = 0.4$ and $\mu = 0.6$; however, the most significant correlation has been observed for $\mu = 0.4$. Accordingly, the value of $\mu = 0.4$ has been used for calculations presented in the paper. We would expect on physical grounds more events to be observed at times when the tidal Coulomb stress has a slip encouraging effect. We also look at the tidal Coulomb stress rate (ΔTCFS) to investigate if there is an increase in seismicity rate at times when the tidal stress accelerates towards its maximum.

3 STATISTICAL TEST

We use the two-rate Poisson model to test the statistical significance of our results (Vidale *et al*. 1998; Gu *et al*. 2008). For fixed sampling frames t_0 and t_1, we count the corresponding number of events x_0 and x_1. Here, t_0 and t_1 refer to the fraction of time with TCFS > 0 (ΔTCFS > 0) and TCFS < 0 (ΔTCFS < 0) and x_0 and x_1 are number of events recorded during the time of positive and negative TCFS (ΔTCFS). In order to determine the sampling time frame t_i for x_i, $i = 0, 1$, we count the number of hours with the positive and negative TCFS (ΔTCFS) for every fault orientation over the investigated period (Fig. 4). Next, we reduce the total time interval to unity so that the sum of a fraction of time t_0 and t_1 is equal to 1. We follow this procedure for the full data set as well as for each specific type of faulting. Taking x_0 and x_1 to be independent Poisson variables, we calculate associated rates γ_0 and γ_1. The maximum likelihood estimate for each rate γ_i is defined by

$$\gamma_i = \frac{x_i}{t_i}, \quad i = 0, 1. \tag{4}$$

Having γ_i for $i = 0, 1$, we proceed by forming the ratio of interest and denoting it as R:

$$R = \frac{\gamma_0}{\gamma_1}. \tag{5}$$

We are interested if the ratio of two rates is equal versus not equal to a pre-specified number R. In effect, we test the following hypotheses:

$$H_0 : \ R = 1 \ \text{ against } H_1 : R \neq 1. \tag{6}$$

The null hypothesis H_0 in (6) is equivalent to the equality of two rates, that is, $\gamma_0 = \gamma_1$ and implies no effect of Earth tides on seismicity rate. On the other hand, the value of $R \neq 1$ under H_1 suggests that tidal stresses acting in a direction favouring Coulomb failure influence the probability of earthquake occurrence. To account for the variability of ratio estimates taken from a limited sample, we construct a $100(1-\alpha)$ % Wald confidence interval (CI) for $R = \gamma_0/\gamma_1$ (Graham *et al*. 2003). Accordingly, the lower limit R_L is given by

$$R_\mathrm{L} = \exp\left(\ln(R) - z_{\alpha/2}\sqrt{\frac{1}{x_0} + \frac{1}{x_1}}\right) \tag{7}$$

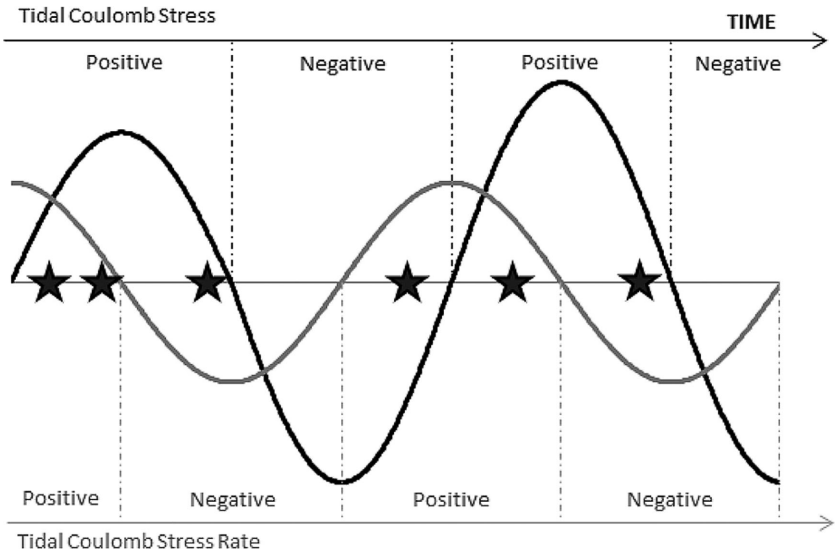

Figure 4. Schematic diagram of time-series of the tidal Coulomb stress (TCFS) and tidal Coulomb stress rate (ΔTCFS). Fractions of time with positive and negative TCFS are marked in black whereas fractions of time with positive and negative ΔTCFS are shown in grey. Stars symbolize hypothetical earthquakes.

and the upper limit is

$$R_{\mathrm{U}} = \exp\left(\ln(R) + z_{\alpha/2}\sqrt{\frac{1}{x_0} + \frac{1}{x_1}}\right). \quad (8)$$

In both eqs (7) and (8), $z_{\alpha/2}$ is a critical value of z for a two-tailed test at the α significance level. A logarithmic transformation is applied for stabilising the variance and skewness correction (Ng & Tang 2005).

Since the test statistics are used to simultaneously evaluate the significance of observations for different case scenarios (see Section 4), we take a conservative approach in defining confidence limits and apply the Bonferroni correction (Zheng *et al*. 2012). This multiple comparison correction technique minimizes the risk of obtaining false positive results by using an adjusted alpha level for each single test. In effect, single threshold values α are calculated in such a way that the family wise error probability p_{FWE} (here adopted $p_{\mathrm{FWE}} = 0.05$) is obtained at the global level. In order to guarantee the family wise error probability of $p_{\mathrm{FWE}} = 1 - (1-\alpha)^n$, the threshold for each considered test is defined by

$$\alpha = 1 - (1 - p_{\mathrm{FWE}})^{1/n}. \quad (9)$$

For small p_{FWE} values (e.g. 0.05), the significance level α can be approximated by simply dividing the family wise error probability p_{FWE} by the n number of independent tests:

$$\alpha = \frac{p_{\mathrm{FWE}}}{n}. \quad (10)$$

Using $z_{p_{\mathrm{FWE}}/2n}$ when constructing n confidence intervals for testing multiple scenarios ensures that all the intervals cover their target parameters simultaneously with 95 per cent confidence (Bland & Altman 1995).

In addition to the ratio estimate, we define the degree of correlation by calculating the percentage of excess events (N_{ex}) during (1) the period of encouraging tidal Coulomb stress (TCFS > 0); (2) the period of encouraging tidal Coulomb stress rate (ΔTCFS > 0). The N_{ex} is given by

$$N_{\mathrm{ex}} = \frac{(x_0 - t_0\, N)\, 100\%}{N}, \quad (11)$$

where x_0 is the number of events recorded during the time of positive tidal Coulomb stress, N is the total number of events and t_0 refers to the fraction of time when TCFS > 0 (or ΔTCFS > 0). Positive values of N_{ex} indicate a surplus of events and negative values, a deficit.

4 RESULTS

We determine the seismicity response to tidal stresses/stress rates and investigate which earthquakes are most prone to tidal triggering (if any) by calculating the ratio estimate R for different case scenarios. The following scenarios are considered:

(1) *ScenarioAll*: x_0 and x_1 correspond to the number of events that occur when TCFS > 0 (ΔTCFS > 0) and TCFS < 0 (ΔTCFS < 0);

(2) *Scenario2h*: x_0 and x_1 correspond to the number of events recorded within the 2 h period centred on the TCFS (ΔTCFS) maxima and minima;

(3) *Scenario3h*: x_0 and x_1 correspond to the number of events recorded within the 3 h period centred on the TCFS (ΔTCFS) maxima and minima.

Our motivation for *Scenario2h* and *Scenario3h* is that the difference in seismicity rates between the encouraging and discouraging tidal phase may be most evident when only events in close proximity to tidal maxima and minima are considered. In fact, the slip-encouraging (tidal maxima) and slip-discouraging effect (tidal minima) are at these times the largest. Since we compare three different case scenarios, simultaneous multiple interval estimates are needed to ensure that the overall confidence coefficient is at least $1 - p_{\mathrm{FWE}}$. The confidence interval for each individual case scenario is thus constructed with confidence coefficient $(1 - \alpha)$ where $\alpha = p_{\mathrm{FWE}}/3$.

Given *ScenarioAll*, we do not observe any significant correlation between tides and earthquakes for any of the studied catalogues (Supporting Information Tables S1–S4). For Catalogues I and II, the estimate of R for either the full data set or a specific fault type has a value above 1, suggesting slight amount of tidal triggering. However, this observation is not found statistically significant as the lower endpoint of the confidence interval extends below 1. In Catalogue III, the estimate of R has a value below 1 for the strike-slip events and the complete data set while in Catalogue IV, the R is marginally above 1 for all fault types but for normal. Also here, the null hypothesis implying the equality of seismicity rates at times of TCFS > 0 and TCFS < 0 cannot be rejected at the α level.

Results of *Scenario2h,* comparing seismicity rates within the 2 h period centred on the TCFS maxima and minima, show that earthquake origin times are non-random for the reverse faults. Accordingly, the rate ratio R is equal to 1.636, 1.492, 1.390 and 1.293 for Catalogues I, II, III and IV, respectively. In all cases, the confidence intervals secure the reliability of ratio estimates meaning that there is less than 1.67 per cent chance that tides and earthquakes are not correlated. For the strike-slip events and the complete data set, we observe increased seismicity rates during times of slip-encouraging tidal stresses; although in both cases R is not found different from 1 at the 98.33 per cent confidence level. Under *Scenario3h*, for which we only consider events recorded within the 3 h period centred on the TCFS maxima and minima, the tidal effect is again detected for the reverse faults. However, the statistically significant tide-earthquake correlation is found only in Catalogue I. Here, the estimate of R has a value of 1.597 and the corresponding confidence bounds of $R_{\mathrm{L}} = 1.084$ and $R_{\mathrm{U}} = 2.353$.

Given *ScenarioAll*, the high percentage of excess events at times of positive tidal Coulomb stresses is found for the reverse faults, that is, 1.54, 1.38 and 7.37 per cent for Catalogues I, II and III respectively. We also report a low percentage of surplus events for the complete data set and strike-slip faults in Catalogues I, II and IV. Under *Scenario2h* and *Scenario3h*, the surplus events are observed for all types of faulting but for normal in four studied catalogues, with the largest value of N_{ex} found in Catalogue I. Again, reverse faults record the highest percentage of excess events during times of encouraging tidal stresses.

Since failures may be more likely to initiate when stress is increasing rather than decreasing, we also investigate the seismicity response to variations of the tidal Coulomb stress rate. Supporting Information Tables S5–S8 show the results of correlation analysis between tidal Coulomb stress rate and earthquake occurrence for Catalogues I, II, III and IV respectively. Under *ScenarioAll,* we observe significant difference between seismicity rates at times of ΔTCFS > 0 and ΔTCFS < 0 for the reverse events in Catalogues I and II. Accordingly, the estimate of ratio has a value of $R = 1.325$ for Catalogue I and $R = 1.245$ for Catalogue II. In both cases the 98.33 per cent confidence interval around the ratio does not extend below 1. The statistically significant tidal effect is also found in Catalogue I given *Scenario3h*. The non-random tidal influence in earthquake timings is however not observed for

the catalogues containing events within 2.5 and 5 km of the nearest faults.

When analysing the number of events at times of positive tidal Coulomb stress rates given *ScenarioAll*, we observe a surplus of strike-slip events in Catalogues I and II, and their deficit in Catalogue III and IV. Furthermore, we find a surplus of reverse events, that is, depending on the catalogue under consideration, from 2.5 per cent to 7.0 per cent more earthquakes is found at $\Delta\mathrm{TCFS} > 0$. Under *Scenario2h* and *Scenario3h*, there are excess events of reverse type in all considered catalogues. The highest percentage of $N_{\mathrm{ex}} = 8.8$ per cent is observed in Catalogue I. Also, in all four catalogues we report surplus events for the normal faults and the full data set. Note that a relatively small sample size of normal fault events may induce a substantial bias into our estimation of N_{ex}.

Since the magnitude, rather than rate, of tidal stresses is found to have more robust correlation with earthquake timings, we test this relationship further. We compute the ratio estimate R for different ranges of the peak tidal Coulomb stress following the methodology of Cochran *et al*. (2004). The peak tidal stress τ_{p} is calculated by averaging the values of stress maxima immediately before and after each earthquake occurrence. To minimize the risk of making false-positive inferences, we construct confidence intervals for a set of 4 different stress magnitude ranges with confidence coefficient $(1-\alpha)$ where $\alpha = p_{\mathrm{FWE}}/4$. We observe that the value of R becomes larger with successively higher amplitudes of the peak tidal stress (Fig. 5). For $\tau_{\mathrm{p}} \geq 1$ kPa, the correlation is the strongest with R of 1.675, 1.616, 1.599 and 1.544 in Catalogues I, II, III and IV, respectively (Table 2). For 0.5 kPa $\geq \tau_{\mathrm{p}} \geq 1.5$ kPa, the seismicity rates are generally higher at $\mathrm{TCFS} > 0$, however, we cannot say that these values are different from 1 at the 98.75 per cent confidence level. In all studied catalogues, the rate ratio R becomes the lowest for $\tau_{\mathrm{p}} < 0.5$ kPa.

Since some studies suggested that earthquakes of smaller magnitude may be more susceptible to tidal stress variations (e.g. Tanaka *et al*. 2002a; Stroup *et al*. 2007), we divide our data set into two categories: events of $M_{\mathrm{w}} < 2.8$ and events of $M_{\mathrm{w}} \geq 2.8$. The magnitude threshold is set so that both samples are comparable in size. Accordingly, Bonferroni-corrected confidence intervals are obtained by using $z_{p\mathrm{FWE}/2n}$ where $n = 2$. For both considered magnitude ranges, the difference in seismicity rates at times of $\mathrm{TCFS} > 0$ and $\mathrm{TCFS} < 0$ is found statistically insignificant and therefore, it is difficult to clearly interpret the effect of earthquake magnitude on the correlation between tides and earthquake timing (Table 3).

5 DISCUSSION

Despite the completely predictable nature of Earth tides and their constant contribution to stress variations in the Earth's crust, the question whether or not tides modulate the timing of earthquakes has given rise to much controversy. Our investigation clearly shows tidal influence in earthquake occurrence, particularly when the differences in seismicity rates near tidal extremes are taken into account.

Under *ScenarioAll*, for which all events are considered, the highest value of R is observed for the reverse fault events in all studied catalogues; although R is not found different from 1 at the 98.33 per cent confidence level. Also, the estimate of R for the full data set and strike slip events (Catalogues I, II and IV) suggests marginal, but not statistically significant, amount of tidal triggering. This finding is consistent with the results presented by Vidale *et al*. (1998). After analysing 13 042 strike-slip events they reported that approximately 1–2 per cent more earthquakes occur at times of slip-encouraging tidal stresses. Despite the higher seismicity rate observed during times when tidal stress promotes failure, they concluded that the statistical significance of the observed excess events could not be confirmed at the 95 per cent confidence level. Furthermore, our observation of larger values of the ratio for the reverse faults, in contrast to strike-slip type (making up approximately 82 per cent of total number of earthquakes) may be attributed to the difference in the amplitude of tidal stress, smaller in the horizontal than vertical direction. Tanaka *et al*. (2002a) compared the amplitude of tidal shear stress on dip-slip and strike-slip faults (assuming the rake and dip angles of 90° and 30° for dip-slip faults, and 0° and 90° for strike-slip faults, respectively) and concluded that that the tidal stress change on dip-slip faults is much larger than that on strike-slip ones.

Results of *Scenario2h*, for which the difference between seismicity rates within the 2 h period centred on the tidal maxima and minima is examined, show that earthquake times are not randomly distributed for the reverse faults. The probability of obtaining this result by chance is less than 1.67 per cent. The correlation for the reverse fault events is found particularly strong in Catalogues I and II, and slightly weaker (but still significant) in Catalogues III and IV. Previously, the non-uniformity in distribution of tidal phase angles for occurrence time of reverse events was observed in studies by Cochran *et al*. (2004) and Tanaka *et al*. (2002a). Cochran *et al*. (2004) found the evidence of tidally induced seismicity when relating timings of 2027 globally distributed shallow thrust earthquakes to the time function of the tidal Coulomb stress. While our analysis includes reverse fault events recorded only in continental regions, Cochran *et al*. (2004) used events from subduction zones characterized by a large ocean-loading component and correspondingly higher amplitudes of stresses. They obtained especially strong correlation for events with the tidal peak Coulomb stress of $\tau_{\mathrm{p}} > 20$ kPa. In the study by Tanaka *et al*. (2002a), the tidal periodicity in timing of 2823 reverse events was found for tidal shear stress. Also here, most of the analysed reverse fault earthquakes occurred near ocean margins where the influence of ocean loading is particularly strong. Due to the fact that reverse fault events used in our investigation are located in continental settings, the maximum amplitude of tidal Coulomb stresses is much lower and corresponds to approximately 5 kPa. It suggests that reverse faulting events may be triggered by even lower amplitudes of stresses then previously assumed.

Given *Scenario3h*, comparing seismicity rates within the 3 h period centred on the tidal maxima and minima, the significant periodicity in timing of earthquakes is again observed for the reverse faults. However, the tidal effect, under assumptions of *Scenario3h*, is generally weaker for either the full data set or a specific focal mechanism compared to one given *Scenario2h*. We therefore conclude that the difference in seismicity rates during times of $\mathrm{TCFS} > 0$ and $\mathrm{TCFS} < 0$ becomes most distinctive when only events in the closest proximity to tidal extremes are considered.

As mentioned in the Methodology section, to minimize selection bias when choosing data set for testing the tide-earthquake correlation, we consider four different catalogues for which events vary with the distance from the failure plane. We observe that for the catalogues including events further away from the principal slip surfaces of late Quaternary faults, the estimate of R becomes gradually lower. One explanation for the decreasing value of R could be a decreasing correlation between the orientation of the mapped structure and that of the actual fault plane for events at a greater distance.

Along with the significant increase in earthquake rates around tidal Coulomb stress maxima, the level of tidal triggering is found

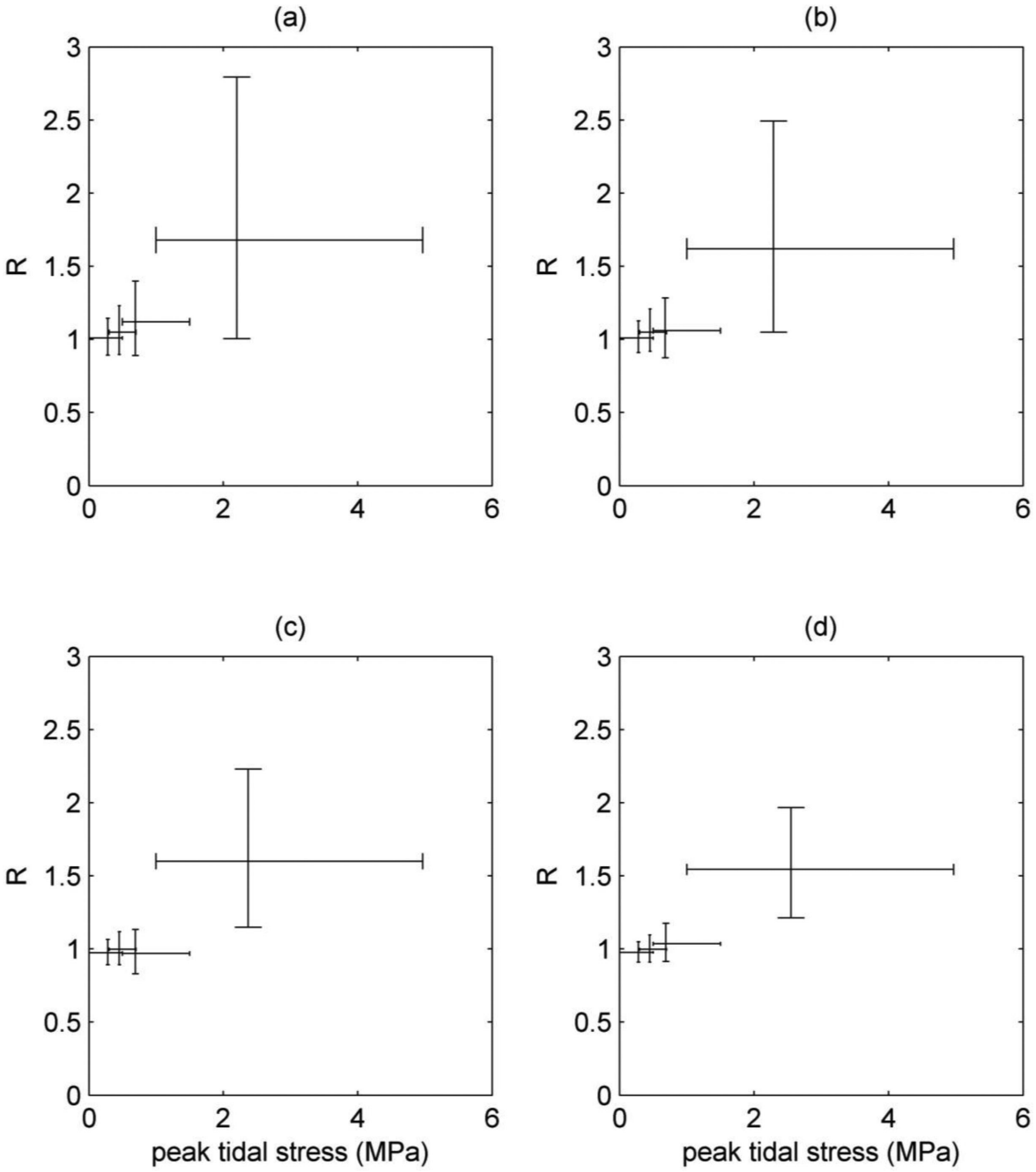

Figure 5. The ratio estimate R versus different ranges of peak tidal Coulomb stress (τ_p) for the (a) Catalogue I; (b) Catalogue II; (c) Catalogue III; (d) Catalogue IV. Values of R with a lower (R_L) and upper (R_U) confidence limits are given in Table 2. Points are located at the mean τ_p. The stress range is indicated by the horizontal lines. Confidence limits are shown by the vertical lines.

to be related to the amplitude of the periodic signal, that is, higher amplitudes of stresses show higher tidal correlations. This appears consistent with both Vidale *et al*. (1998) who observed little triggering of earthquakes by tides in central California and Cochran *et al*. (2004) who found notable triggering in regions of large tidal stress. Also, this finding is in agreement with the results of the laboratory experiment conducted by Lockner & Beeler (1999). They showed that sequences of 20 stick-slip events at a confining pressure of 50×10^3 kPa become correlated with an imposed periodic load, once the amplitude of the load exceeds 100 kPa**.** Furthermore, they claimed that for amplitudes below 6 kPa, little or no correlation can be detected. Our observation, however, provides evidence that the correlation of earthquake timings can clearly be significant for tidal Coulomb stress amplitudes below given detection threshold (Table 2). This might suggest that while the laboratory-derived measurements of triggering by stress loads are set in completely dry environment, the enhanced level of tide-earthquake correlation on the natural faults can be partially contributed to the presence of fluid-filled cracks. The stronger responsiveness of faults to smaller stress loads could also be due to complex fault structure or differences in the perturbation period.

When comparing seismicity rates during times of tidal stress increase and decrease, we observe significantly more events of reverse

Table 2. Data summary is shown for different amplitudes of peak tidal Coulomb stress ranges (τ_p). N is the number of events in each τ_p bin, R is the ratio of two Poisson rates, and R_L and R_U are the lower and upper limit of the constructed confidence interval. Statistical analysis has been conducted for the four earthquake catalogues described in Section 2. Ratios in bold indicate correlations significant at the 98.75 per cent confidence level. The $\mu = 0.4$ is used for calculating tidal stresses.

Distance from the fault (m)	τ_p (kPa)	N	R_L	R	R_U
1000	<0.5	1625	0.892	1.010	1.144
	$0.3 \leq \tau_p < 0.7$	1007	0.897	1.050	1.230
	$0.5 \leq \tau_p < 1.5$	491	0.890	1.115	1.397
	≥1	98	**1.004**	**1.675**	**2.794**
1500	<0.5	2198	0.910	1.012	1.127
	$0.3 \leq \tau_p < 0.7$	1334	0.918	1.053	1.208
	$0.5 \leq \tau_p < 1.5$	685	0.875	1.060	1.283
	≥1	136	**1.048**	**1.616**	**2.492**
2500	<0.5	3241	0.891	0.974	1.063
	$0.3 \leq \tau_p < 0.7$	1973	0.891	0.998	1.117
	$0.5 \leq \tau_p < 1.5$	1038	0.830	0.970	1.133
	≥1	231	**1.147**	**1.599**	**2.229**
5000	<0.5	4902	0.910	0.977	1.050
	$0.3 \leq \tau_p < 0.7$	2924	0.910	0.998	1.095
	$0.5 \leq \tau_p < 1.5$	1586	0.913	1.036	1.175
	≥1	433	**1.212**	**1.544**	**1.967**

Table 3. Comparison of the two-rate ratios for different earthquake magnitude ranges. The ratio R is calculated for sampling frames TCFS > 0 and TCFS < 0. x_0 and x_1: correspond to the number of events that occur for TCFS > 0 and TCFS < 0 (*ScenarioAll*). N is the total number of events. N_{ex} is the percentage of excess events. R is the ratio of two Poisson rates with R_L and R_U defined as the lower and upper confidence limits, respectively. Statistical analysis has been conducted for the four earthquake catalogues described in Section 2. The $\mu = 0.4$ is used for calculating tidal stresses.

	$M_w < 2.8$					$M_w \geq 2.8$				
	N	N_{ex}	R_L	R	R_U	N	N_{ex}	R_L	R	R_U
Catalogue I										
All	1022	1.53	0.92	1.06	1.22	1171	0.75	0.90	1.03	1.18
Strike	832	0.82	0.88	1.03	1.21	958	1.12	0.90	1.05	1.21
Reverse	183	4.37	0.85	1.19	1.66	197	−1.84	0.67	0.93	1.28
Normal	7	1.66	0.19	1.07	5.93	16	15.22	0.60	1.85	5.72
Catalogue II										
All	1385	1.00	0.92	1.04	1.17	1605	0.87	0.93	1.04	1.16
Strike	1137	0.46	0.89	1.02	1.16	1317	1.23	0.93	1.05	1.19
Reverse	232	3.64	0.86	1.16	1.55	271	−1.29	0.72	0.95	1.25
Normal	16	−3.70	0.27	0.86	2.72	17	11.79	0.54	1.61	4.78
Catalogue III										
All	2077	−0.40	0.89	0.98	1.09	2392	0.02	0.91	1.00	1.10
Strike	1700	−0.89	0.86	0.96	1.08	1948	0.02	0.90	1.00	1.11
Reverse	350	1.91	0.85	1.08	1.37	416	−0.25	0.79	0.99	1.23
Normal	27	−4.18	0.34	0.84	2.05	28	8.81	0.61	1.43	3.33
Catalogue IV										
All	3233	−0.76	0.90	0.97	1.05	3624	−0.12	0.92	1.00	1.07
Strike	2645	−1.04	0.88	0.96	1.05	2922	0.03	0.92	1.00	1.09
Reverse	537	1.53	0.88	1.06	1.29	638	−0.89	0.81	0.96	1.15
Normal	51	−5.97	0.40	0.78	1.50	64	−0.63	0.55	0.97	1.72

type at ΔTCFS > 0 in Catalogues I and II. While the periodicity in earthquake timing for the tidal stress is observed in all four catalogues, the correlation between tidal stress rate and earthquake occurrence is not seen in catalogues containing events within 2.5 and 5 km of the nearest faults which makes it more difficult to interpret. In fact, this study is not the first that finds a stronger correlation for tidal stress rather than stressing rate. Thomas *et al.* (2009) show that correlation between tremor occurrence and tidal stress rate is insignificant for all stress components (i.e. normal, shear and Coulomb). At the same time, they demonstrate that the tremor surpluses and deficits, depending on the loading conditions under which they occur, are most pronounced for the tidal Coulomb and shear stresses.

We cannot conclude with certainty for which of two investigated earthquake magnitude ranges the tidal signal is more distinctive. The ratio R for both groups in all studied catalogues is not found different from 1 at the Bonferroni-corrected 97.5 per cent confidence level. Therefore, the similar response to tidal

stress perturbations of events of different magnitude may support the viewpoint that the nucleation processes of small and large earthquakes do not differ (e.g. Abercrombie & Mori 1994; Steacy & McCloskey 1998).

6 CONCLUSIONS

We systematically examine the correlation between the tidal Coulomb stress/stress rate and earthquake occurrence using four Southern California earthquake catalogues. Each catalogue consists of events with varying distance from the failure plane that is assumed to be controlled by the orientation of the nearest adjacent fault. The results we obtain show a significant increase in earthquake rates within the 2 h (*Scenario2h*) and 3 h (*Scenario3h*) period centred on the tidal maxima for the reverse events. The increased rates of seismicity are in fact higher than those predicted by laboratory simulations of fault failure under periodic loading (Lockner & Beeler 1999). We do not observe any significant correlation between tides and earthquakes for any of the studied catalogues when all earthquakes are considered (*ScenarioAll*). We also show that the magnitude of stress change plays an important role in tidal triggering. First, the tidal effect appears weaker for results obtained under assumptions of *Scenario3h* than *Scenario2h* and second, the level of tidal triggering is shown to be related to the amplitude of the peak tidal Coulomb stress. Finally, it should be noted that despite the fact that a significant tidal signal is observed for certain case scenarios or data sets, its influence on actual earthquake rates is very small.

7 DATA AND RESOURCES

The earthquake data are obtained from the Southern California Earthquake Data Center (http://www.data.scec.org/index.html). The fault parameters are taken from the *Probabilistic Seismic Hazard Assessment for the State of California* open-report (http://www.consrv.ca.gov/) and *Documentation for the 2008 Update of the United States National Seismic Hazard Maps* (http://pubs.er.usgs.gov/). The Reasenberg's algorithm used in this study is included in the ZMAP package for MATLAB (Wiemer 2001) that can be freely downloaded from the Swiss Seismological Service website (http://www.seismo.ethz.ch/prod/software/).

ACKNOWLEDGEMENTS

We would like to thank the Editor Duncan Agnew, second Editor, Dr Guillaume Daniel, and two anonymous reviewers for their helpful comments. The project was supported by the Department for Employment and Learning, Northern Ireland.

REFERENCES

Abercrombie, R.E. & Mori, J., 1994. Local observations of a large earthquake: 28 June 1992, Landers, California, *Bull. seism. Soc. Am.,* **84,** 725–734.

Agnew, D.C., 2012. SPOTL: some programs for ocean-tide loading, in *SIO Tech. Rep. Scripps Inst. Oceanogr.,* Univ. of Calif., La Jolla.

Ashtari Jafari, M., 2010. Statistical prediction of the next great earthquake around Tehran, Iran, *J. Geodyn.,* **49**(1), 14–18.

Ayyub, B.M. & McCuen, R.H., 2011. *Probability, Statistics, and Reliability for Engineers and Scientists,* 3rd edn, CRC Press.

Bland, J.M. & Altman, D.G., 1995. Multiple significance tests: the Bonferroni method, *BMJ,* **310,** 170, doi:10.1136/bmj.310.6973.170.

Chernick, M.R., 2007. *Bootstrap Methods: A Guide for Practitioners and Researchers,* 2nd edn, Wiley-Interscience.

Cochran, E.S., Vidale, J.E. & Tanaka, S., 2004. Earth tides can trigger shallow thrust fault earthquakes, *Science,* **306,** 1164–1166.

Curchin, J.M. & Pennington, W.D., 1987. Tidal triggering of intermediate and deep focus earthquakes, *J. geophys. Res.,* **92,** 13 957–13 967.

Emter, C., 1997. Tidal triggering of earthquakes and volcanic events, in *Tidal Phenomena, Lecture Notes in Earth Sciences,* Vol. 66, pp. 293–310, eds Wilhem, H., Zürn, W. & Wenzel, H.-G., Springer-Verlag.

Freed, A.M. & Lin, J., 2001. Delayed triggering of the 1999 Hector Mine earthquake by viscoelastic stress transfer, *Nature,* **411,** 180–183.

Gardner, J.K. & Knopoff, L., 1974. Is the sequence of earthquakes in Southern California, with aftershocks removed, Poissonian?, *Bull. seism. Soc. Am.,* **64**(5), 1363–1367.

Gomberg, J., 1996. Stress/strain changes and triggered seismicity following the M_w 7.3 Landers, California, earthquake, *J. geophys. Res.,* **101,** 751–764.

Gomberg, J., Reasenberg, P.A., Bodin, P. & Harris, R., 2001. Earthquakes triggering by seismic waves following the Landers and Hector mine earthquakes, *Nature,* **411,** 462–465.

Gomberg, J., Bodin, P., Larson, K. & Dragert, H., 2004. Earthquake nucleation by transient deformations caused by the M = 7.9 Denali, Alaska, earthquake, *Nature,* **427,** 621–624.

Gonzalez-Huizar, H., Velasco, A.A., Peng, Z. & Castro, R.R., 2012. Remote triggered seismicity caused by the 2011 M9.0 Tohoku-Oki, Japan earthquake, *Geophys. Res. Lett.,* **39,** L10302, doi:10.1029/2012GL051015.

Graham, P.L., Mengersen, K. & Morton, A.P., 2003. Confidence limits for the ratio of two rates based on likelihood scores: non-iterative method, *Stat. Med.,* **22,** 2071–2083.

Gu, K., Ng, H.K.T., Tang, M.L. & Schucany, W.R., 2008. Testing the Ratio of Two Poisson Rates, *Biome. J.,* **50,** 2831–298.

Hardebeck, J.L., Nazareth, J.J. & Hauksson, E., 1998. The static stress change triggering model: constraints from two southern California aftershock sequences, *J. geophys. Res.,* **103,** 24 427–24 437.

Hartzell, S. & Heaton, T., 1989. The fortnightly tide and the tidal triggering of earthquakes, *Bull. seism. Soc. Am.,* **79,** 1282–1286.

Heaton, T.H., 1982. Tidal triggering of earthquakes, *Bull. seism. Soc. Am.,* **72,** 2180–2200.

Hill, D.P. & Prejean, S., 2013. Dynamic triggering, in *V. 4 Earthquake Seismology, Treatise on Geophysics,* 2nd edn, ed. Kanamori, H., Elsevier.

Iwata, T., 2002. Tidal stress/strain and acoustic emission activity at the underground research laboratory, Canada, *Geophys. Res. Lett.,* **29,** 30-1–30-4.

Iwata, T. & Young, R.P., 2005. Tidal stress/strain and the *b*-values of acoustic emissions at the Underground Research Laboratory, Canada, *Pure appl. Geophys.,* **162,** 1291–1308.

Kagan, Y.Y. & Jackson, D.D., 1991. Long-term earthquake clustering, *Geophys. J. Int.,* **104,** 117–134.

King, G.C.P., Stein, R.S. & Lin, J., 1994. Static stress changes and the triggering of earthquakes, *Bull. seism. Soc. Am.,* **84,** 935–953.

Lasocki, S., Karakostas, V.G. & Papadimitriou, E.E., 2009. Assessing the role of stress transfer on aftershock locations, *J. geophys. Res.,* **114,** B11304, doi:10.1029/2008JB006022.

Lockner, D.A. & Beeler, N.M., 1999. Premonitory slip and tidal triggering of earthquakes, *J. geophys. Res.,* **104,** 20 133–20 151.

Matsumoto, K., Takanezawa, T. & Ooe, M., 2000. Ocean tide models developed by assimilating TOPEX/POSEIDON altimeter data into hydrodynamical model: a global model and a regional model around Japan, *J. Oceanogr.,* **56,** 567–581.

Matsumoto, K., Sato, T., Takanezasa, T. & Ooe, M., 2001. GOTIC2: a program for computation of oceanic tidal loading effect, *J. Geod. Soc. Japan,* **47,** 243–248.

Métivier, L., de Viron, O., Conrad, C.P., Renault, S., Diamen, M. & Patau, G., 2009. Evidence of earthquake triggering by the solid earth tides, *Earth planet. Sci. Lett.,* **278,** 370–375.

Mignan, A., Werner, M.J., Wiemer, S., Chen, C.-C. & Wu, Y.-M., 2011. Bayesian estimation of the spatially varying completeness magnitude of earthquake catalogs, *Bull. seism. Soc. Am.,* **101,** doi:10.1785/0120100223.

Ng, H.K.T. & Tang, M.L., 2005. Testing the equality of two Poisson means using the rate ratio, *Stat. Med.,* **24,** 955–965.

Petersen, M.D., Bryant, W.A., Cramer, Ch.H., Cao, T. & Reichle, M., 1996. *Probabilistic Seismic Hazard Assessment for the State of California,* California Department of Conservation, Division of Mines and Geology.

Petersen, M.D. *et al.*, 2008. *Documentation for the 2008 Update of the United States National Seismic Hazard Maps,* U.S. Department of the Interior, U.S. Geological Survey.

Pollitz, F.F. & Sacks, I.S., 2002. Stress triggering of the 1999 Hector Mine earthquake by transient deformation following the 1992 Landers earthquake, *Bull. seism. Soc. Am.,* **92,** 1487–1496.

Ranalli, G., 1995. *Rheology of the Earth,* 2nd edn, Chapman and Hall.

Reasenberg, P., 1985. Second-order moment of central California seismicity, 1969–1982, *J. geophys. Res.,* **90**(B7), 5479–5495.

Scholz, Ch.H., 2002. *The Mechanics of Earthquakes and Faulting,* Cambridge Univ. Press.

Shirley, J.H., 1988. Lunar and solar periodicities of large earthquakes: Southern California and the Alaska-Aleutian Islands seismic region, *Geophys. J. Int,* **92,** 403–420.

Steacy, S.J. & McCloskey, J., 1998. What controls an earthquake's size? Results from a heterogeneous cellular automaton, *Geophys. J. Int,* **133**(1), F11–F14.

Stein, R.S., Barka, A.A. & Dieterich, J.H., 1997. Progressive failure on the North Anatolian fault since 1939 by earthquake stress triggering, *Geophys. J. Int.,* **128,** 594–604.

Stroup, D.F., Bohnenstiehl, D.R., Tolstoy, M., Waldhauser, F. & Weekly, R.T., 2007. Pulse of the seafloor: tidal triggering of microearthquakes at 9°50′N East Pacific Rise, *Geophys. Res. Lett.,* **34,** L15301, doi:10.1029/2007GL030088.

Takanezawa, T., Matsumoto, K., Ooe, M. & Naito, I., 2001. Effects of the period ocean tides on Earth rotation, gravity and crustal deformation predicted by global barotropic model—Period from Mtm to Sa, *J. Geod. Soc. Japan,* **47,** 545–550.

Tanaka, S., 2012. Tidal triggering of earthquakes prior to the 2011 Tohoku-Oki earthquake (M_w 9.1), *Geophys. Res. Lett.,* **39,** L00G26, doi:10.1029/2012gl051179.

Tanaka, S., Ohtake, M. & Sato, H., 2002a. Evidence for tidal triggering of earthquakes as revealed from statistical analysis of global data, *J. geophys. Res.,* **107**(B10), ESE 1-1–ESE 1-11.

Tanaka, S., Ohtake, M. & Sato, H., 2002b. Spatio-temporal variation of the tidal triggering effect on earthquake occurrence associated with the 1982 South Tonga earthquake of M_w 7.5, *Geophys. Res. Lett.,* **29**(16), 3-1–3-4.

Tanaka, S., Ohtake, M. & Sato, H., 2004. Tidal triggering of earthquakes in Japan related to the regional tectonic stress, *Earth Planet. Space,* **56,** 511–515.

Thomas, A.M., Nadeau, R.M. & Burgmann, R., 2009. Tremor-tide correlations and near-lithostatic pore pressure on the deep San Andreas fault, *Nature,* **462**(7276), 1048–1051.

Tsuruoka, H., Ohtake, M. & Sato, H., 1995. Statistical test of the tidal triggering of earthquakes: contribution of the ocean tide loading effect, *Geophys. J. Int.,* **122,** 183–194.

Vidale, J.E., Agnew, D.C., Johnston, M.J.S. & Oppenheimer, D.H., 1998. Absence of earthquake correlation with Earth tides: an indication of high preseimic fault stress rate, *J. geophys. Res.,* **103,** 24 567–24 572.

Wang, J.P., Lin, C.W., Taheri, H. & Chen, W.S., 2012. Impact of fault parameter uncertainties on earthquake recurrence probability by Monte Carlo simulation – an example in central Taiwan, *Eng. Geol.,* **126,** 67–74.

Wenzel, H.-G., 1996. The nanogal software: Earth tide data processing package ETERNA 3.30, *Bull. d'Informations Mareés Terrestres,* **124,** 9425–9439.

West, M., Sanchez, J.J. & McNutt, S.R., 2005. Periodically triggered seismicity at Mount Wrangell, Alaska, after the Sumatra earthquake, *Science,* **308,** 1144–1146.

Wiemer, S., 2001. A software package to analyze seismicity: ZMAP, *Seismol. Res. Lett.,* **92,** 373–382.

Wiemer, S. & Wyss, M., 2000. Minimum magnitude of complete reporting in earthquake catalogs: examples from Alaska, the western United States, and Japan, *Bull. seism. Soc. Am.,* **90,** 859–869.

Wilcock, W.S.D., 2001. Tidal triggering of microearthquakes on the Juan de Fuca Ridge, *Geophys. Res. Lett.,* **28,** 3999–4002.

Wilcock, W.S.D., 2009. Tidal triggering of earthquakes in the Northeast Pacific Ocean, *Geophys. J. Int.,* **179,** 1055–1070.

Yang, W., Hauksson, E. & Shearer, P.M., 2012. Computing a large refined catalog of focal mechanisms for Southern California (1981–2010): temporal stability of the style of faulting, *Bull. seism. Soc. Am.,* **102,** 1179–1194.

Zheng, G, Yang, Y., Zhu, X. & Elston, R.C., 2012. *Analysis of Genetic Association Studies,* Springer Science & Business Media.

Zhuang, J., Ogata, Y. & Vere-Jones, D., 2002. Stochastic declustering of space-time earthquake occurrences, *J. Am. Stat. Assoc.,* **97,** 369–380.

SUPPORTING INFORMATION

Additional Supporting Information may be found in the online version of this paper:

Table S1. Results of the statistical test for tidal Coulomb stress (TCFS) given the Catalogue I. *t0* is the fraction of time with TCFS > 0. *x0* and *x1*: (1) correspond to the number of events that occur for TCFS > 0 and TCFS < 0 (*ScenarioAll*); (2) correspond to the number of events recorded within the 2 hr period centred on the TCFS maxima and minima (*Scenario2h*); (3) correspond to the number of events recorded within the 3 hr period centred on the TCFS maxima and minima (*Scenario3h*). N is the total number of events. N_{ex} is the percentage of excess events. R is the ratio of two Poisson rates with R_L and R_U defined as the lower and upper confidence limits, respectively. Ratios in bold indicate correlations significant at the 98.33 per cent confidence level. The $\mu = 0.4$ is used for calculating TCFS.

Table S2. Results of the statistical test for tidal Coulomb stress given the Catalogue II. The notations used are described in Table S1. Ratios in bold indicate correlations significant at the 98.33 per cent confidence level. The $\mu = 0.4$ is used for calculating TCFS.

Table S3. Results of the statistical test for tidal Coulomb stress given the Catalogue III. The notations used are described in Table S1. Ratios in bold indicate correlations significant at the 98.33 per cent confidence level. The $\mu = 0.4$ is used for calculating TCFS.

Table S4. Results of the statistical test for tidal Coulomb stress given the Catalogue IV. The notations used are described in Table S1. Ratios in bold indicate correlations significant at the 98.33 per cent confidence level. The $\mu = 0.4$ is used for calculating TCFS.

Table S5. Results of the statistical test for tidal Coulomb stress rate (ΔTCFS) given the Catalogue I. *t0* is the fraction of time with ΔTCFS > 0. *x0* and *x1*: (1) correspond to the number of events that occur for ΔTCFS > 0 and ΔTCFS < 0 (*ScenarioAll*); (2) correspond to the number of events recorded within the 2 hr period centred on the ΔTCFS maxima and minima (*Scenario2h*); (3) correspond to the number of events recorded within the 3 hr period centred on the ΔTCFS maxima and minima (*Scenario3h*). N is the total number of events. N_{ex} is the percentage of excess events. R is the ratio of two Poisson rates with R_L and R_U defined as the lower and upper confidence limits, respectively. Ratios in bold indicate correlations significant at the 98.33 per cent confidence level. The $\mu = 0.4$ is used for calculating ΔTCFS.

Table S6. Results of the statistical test for tidal Coulomb stress rate given the Catalogue II. The notations used are described in

Table S5. Ratios in bold indicate correlations significant at the 98.33 per cent confidence level. The $\mu = 0.4$ is used for calculating ΔTCFS.

Table S7. Results of the statistical test for tidal Coulomb stress rate given the Catalogue III. The notations used are described in Table S5. The $\mu = 0.4$ is used for calculating ΔTCFS.

Table S8. Results of the statistical test for tidal Coulomb stress rate given the Catalogue IV. The notations used are described in Table S5. The $\mu = 0.4$ is used for calculating ΔTCFS (http://gji.oxfordjournals.org/lookup/suppl/doi:10.1093/gji/ggw045/-/DC1).

Please note: Oxford University Press is not responsible for the content or functionality of any supporting materials supplied by the authors. Any queries (other than missing material) should be directed to the corresponding author for the paper.